Journal of Hydrology 595 (2021) 125658

Contents lists available at ScienceDirect

Journal of Hydrology

journal homepage: www.elsevier.com/locate/jhydrol

Research papers

DOC and nitrate fluxes from farmland; impact on a dolostone aquifer KCZ

G. Medici [a,*], P. Baják [b], L.J. West [c], P.J. Chapman [d], S.A. Banwart [c]

[a] G360 Institute of Groundwater Research, University of Guelph, Stone Road, Guelph, Ontario N1G 2W1, Canada
[b] József and Erzsébet Tóth Endowed Hydrogeology Chair, Institute of Geography and Earth Sciences, Eötvös Loránd University, Pázmány Péter Sétány, Budapest 1117, Hungary
[c] School of Earth and Environment, University of Leeds, Woodhouse Lane, Leeds, W Yorkshire LS2 9JT, UK
[d] Water@leeds, School of Geography, University of Leeds, Woodhouse Lane, Leeds, W Yorkshire LS2 9JT, UK

ARTICLE INFO

This manuscript was handled by Corradini, Editor-in-Chief

Keywords:
Karst Critical Zone
Farmland
DOC
Nitrate
Mass Flux
Contaminant Transport

ABSTRACT

DOC and nitrate in farmland represent key chemical species that determine the water quality in the Karst Critical Zone (KCZ). The work reported here focuses on quantifying fluxes of these species in an experimental farm site (University of Leeds Farm, UK) overlying a dolomitic karst aquifer of Permian age. In this research, the Transect Method was applied for the first time to farmland by combining hydrochemical data from soil and groundwater for computation of mass fluxes. The Transect Method, developed for management of industrially contaminated sites, was applied to a farm source due to the presence of localised contamination from application of pig slurry.

Required inputs for our approach include concentrations of nitrate and DOC in soil water and groundwater, net recharge flux (here derived from a MODFLOW-2005 model) and local hydraulic gradient and conductivity measurements. Key outputs are fluxes and downstream groundwater concentrations of DOC and nitrate. Downstream concentrations were validated against direct groundwater measurements, demonstrating the veracity of the approach. The approach shows that the localised contamination has a significant impact on both concentrations of nitrate and DOC in groundwater, although the DOC impact is greater, because the upstream land uses also produce nitrate as a result of agricultural practices that are widespread in the region.

The results of the study also constrain the zone vulnerable to contamination to the upper ~40 m below the ground surface. Future modelling efforts on solute contaminant transport should focus on this shallow vulnerability zone (0–40 mBGL) and the Transect Method applied in this work can be used to define boundary conditions.

Hence, following this research, we envisage to export a generic approach that combines physical flow parameters and hydrochemical analyses for computation of subsurface mass fluxes using the Transect Method, to identify the degree of impact of specific point sources and to support conceptualization and modelling of contaminant transport in the KCZ of farm areas.

1. Introduction

The Critical Zone is the thin surface layer that extends from the top of the vegetation to the bottom of active groundwater circulation driven by meteorological recharge and supplies humans with most life-sustaining resources (Banwart et al., 2011, 2017; Anderson et al., 2014; Brantley et al., 2017; Keller, 2019). Karst aquifers of carbonate origin represent a source of drinking water that supplies a quarter of the world's population (Ford and Williams, 1989; Hartmann et al., 2014). This category of fractured aquifers is particularly prone to dissolution that enlarges bedding planes, fractures and faults. Consequently, karst aquifers are characterized by a high degree of hydraulic connectivity with the land surface and transport of contaminants is therefore particularly rapid (Ford and Williams, 1989; Worthington et al., 2012; Goldscheider and Drew, 2014; Medici et al., 2016; Borović et al., 2019; Torresan et al., 2020). The Critical Zone in karst environment is considered as the most vulnerable to contamination due to the above mentioned dissolution processes in the vadose and shallow saturated zone of carbonate aquifers (Lian et al., 2011; Kogovsek and Petric, 2014; Zhang et al., 2017; Jiang et al., 2019; Jourde et al., 2018; Green et al., 2019; Sullivan et al., 2019). Stress on groundwater resources of the KCZ has increased in recent decades in agricultural areas in terms of (i) quantity due to excessive

* Corresponding author.
E-mail address: giacomo.medici@g360group.org (G. Medici).

https://doi.org/10.1016/j.jhydrol.2020.125658

Available online 22 October 2020

abstraction of groundwater for irrigation, and (ii) water quality due to pollution from agricultural practices (Mahler and Massei, 2007; Bicalho et al., 2012; Huebsch et al., 2013; Goldscheider and Drew, 2014; Hartmann et al., 2014). The research presented in this paper focuses on the second aspect of interest to the KCZ international community that is represented by protection of water resources from contamination.

Applications of N-fertilizer and manure have increased crop yields while also increasing nitrate concentrations in ground and surface water. For example, Defra (2002) estimated that between 70 and 80% of nitrate in English surface and groundwater derives from agricultural activities. Other sources of nitrate include atmospheric deposition, discharge from septic tanks and leaking sewers, the spreading of sewage sludge to land and seepage from landfills (Wakida and Lerner, 2005; Fezzi et al., 2010; Hutchins, 2012). Elevated nitrate in groundwater has implications for human health. Therefore, quantification of nitrate fluxes in the unsaturated zone and groundwater across agricultural areas is a key element of managing water resources. However, few studies have effectively integrated water quality data and hydrogeological information to estimate fluxes of nitrate, or other pollutants, from agricultural soils to the unsaturated zone and shallow groundwater (Liao et al., 2012; Green et al., 2018). To integrate these research areas dedicated to nitrate pollution, we present a baseline hydro-chemical analysis of soil and groundwater water which we use to compute both DOC and nitrate mass fluxes for the University of Leeds (UoL) Farm, UK (Fig. 1a–c).

The amount of nitrate available for leaching from the soil is related to the amount, timing and method of application of inorganic fertilizers, slurry and/or farmyard manure to agricultural land (Foster, 1976; Sieling et al., 1997; Lord et al., 1999; Williams and Gresham, 2000; Wang et al., 2016). Furthermore, the rate of nitrate leaching through the soil is controlled by texture, with sandy soils allowing more leaching through larger better connected pore spaces than clay rich soils (Goss et al., 1998). The fraction of applied nitrogen that is actually leached to groundwater (“leaching fraction’’) from the soil zone is a key parameter linking nitrogen applications to groundwater nitrate concentrations and typically ranges between 5% and 50% (Liao et al., 2012; Green et al., 2018). Nitrate leaching will also depend on the extent of denitrification within the soil zone, which is function of the nitrate and DOC concentrations, fluid temperature, pH and alkalinity and is therefore strongly dependant on the characteristics of the study site (Panno et al., 2001; Rivett et al., 2008; Mellander et al., 2012; Yang et al., 2020). Denitrification in groundwater in limestone aquifers can also occur (Panno et al., 2001) but is likely to be limited at our field site due to relatively low temperatures, dolostone lithology and rapid fracture flow (Rivett et al., 2008; Moon et al, 2006). Furthermore, Siemens et al. (2003) found in their study that DOC leached from agricultural soils contributed negligibly to the denitrification of nitrate in groundwater because the DOC derived from the soil was not bio-available. Toxic hydrophobic organic contaminants are released by pesticides and form complexes with DOC that facilitates their transport through the soil to the aquifer below (Huang et al., 1998; Weber et al., 1998; Wang et al., 2004, 2016, 2018). Given the role of DOC in influencing both sorption and biodegradation process its importance in influencing groundwater chemistry has been increasingly recognised (Allen-King et al., 2002). Hence, detection of the most vulnerable aquifer zone to infiltration and transport of both DOC and nitrate is included in this research.

To date, the Critical Zone scientific network has primary focused on weathering processes and the geochemical properties of soil and vadose zone using laboratory experimental and modelling approaches (e.g., Emblanch et al., 2003; Falcone et al., 2008; Peyraube et al., 2012, 2013; Dong et al., 2018; Lerch et al., 2018; Zhou et al., 2019; Tremosa et al., 2020). Consequently, there is need for more field scale monitoring and hydraulic testing to characterize the unsaturated and saturated zone as recently highlighted by Critical Zone scientists Kuntz et al. (2011) and Jourde et al. (2018), and shown in this work.

Previous hydrogeological research at the UoL Farm consists of multi-level slug tests (Medici et al., 2019a), pumping tests (Allen et al., 1997) and development of a regional scale steady state MODFLOW-2005 groundwater flow model (Medici et al., 2019b) of the local dolostone aquifer of Permian age. The three formations (Cadeby, Edlington and Brotherton illustrated in Fig. 1c) of the Mangnesian Limestone Group represents separate layers in the model. This groundwater flow model accounts for turbulent flow by inserting the Conduit Flow Process Type-1 (*sensu* Hill et al., 2010) developed by the USGS for karst systems in correspondence of streams and normal faults. Indeed, transmissivities from pumping tests in correspondence of streams and faults is one order of magnitude higher than the host rock due to the presence of karst conduits 0.10–0.20 m large of approximate pipe shape (Medici et al., 2019b). This modelling research has produced calibrated recharge and hydraulic conductivity values that represent inputs for the workflow presented here (Medici et al., 2019a, 2019b).

Nitrate and DOC represent two chemical species, which are considered diagnostic of water quality pollution in karst environments in areas of the world characterized by intense agricultural activities (Ryan and Meiman, 1996; Lastennet and Mudry, 1997; Goldscheider and Drew, 2014). The aim of this research is therefore to show how the combination of groundwater hydrological fluxes with soil water chemistry, baseline groundwater hydrochemistry and monitoring supports reliable computation of DOC and nitrate fluxes from specific agricultural activities which represent point source inputs, developing a method that can be applied in other farmlands overlying KCZs. The specific research objectives were: (i) determine baseline hydrochemical analysis of soil, spring and stream water and groundwater in the KCZ under the UoL Farm, (ii) detect depth of penetration of farm-derived nitrate and DOC in the sub-surface, and (iii) compute and validate nitrate and DOC mass fluxes and downstream concentrations in groundwater in an area of farming activity.

2. Field site

2.1. Bedrock geology

The experimental site of the UoL Farm (see Figs. 1a-d, 2) is located in Yorkshire (NE England, UK) between the cities of Leeds and York. Here, the Magnesian Limestone Group represents the major aquifer and the bedrock lithology. This geological group of Lower Permian age is comprised of dolomitic limestone, dolostone, halite and gypsum rocks derived from shallow water sedimentation at the margins of the Zechstein Basin (Fig. 1a; Aldrick, 1978; Smith et al., 1986). In NE England, the stratigraphic succession of the Magnesian Limestone Group is typically 120 m thick (Cooper and Lawley, 2007). This geological group is formally sub-divided into three different formations: the Cadeby, Edlington and Brotherton formations (Fig. 2a; Smith et al., 1986). The Cadeby Formation that represents the focus of this research is characterized, with the exception of the basal 5 m of marls, by thinly bedded dolostone showing ooids, peloids, corals and bivalves (Tucker, 1991; Mawson and Tucker, 2009). The Brotherton Formation above represents the uppermost part of the Magnesian Limestone Group in Yorkshire and is characterized by thinly bedded dolomitic limestones with ooids, algae and bivalves. However, the Edlington Formation is characterized by both halite and gypsum (Smith et al., 1986).

Higher dolomitisation characterizes the Cadeby Formation (54% $CaCO_3$; 46% $MgCO_3$) that represents the focus of this study. In contrast, the dolomitic limestone of the Brotherton Formation is more abundant in calcite (65% $CaCO_3$; 35% $MgCO_3$), hence more prone to dissolution and permeability development (Allen et al., 1997; Lott and Cooper, 2005). In NE England around the area of study (Figs. 1c, 2a), the tectonic structures which characterize the UK Magnesian Limestone Group are represented by normal faults and non-stratabound joints (*sensu* Odling et al., 1999). Outcrop studies and seismic lines carried out near the field site show how normal faults of Mesozoic age are mainly oriented ENE-WSW (Figs. 1c, 2a). Lack of significant effects of the Cenozoic Alpine

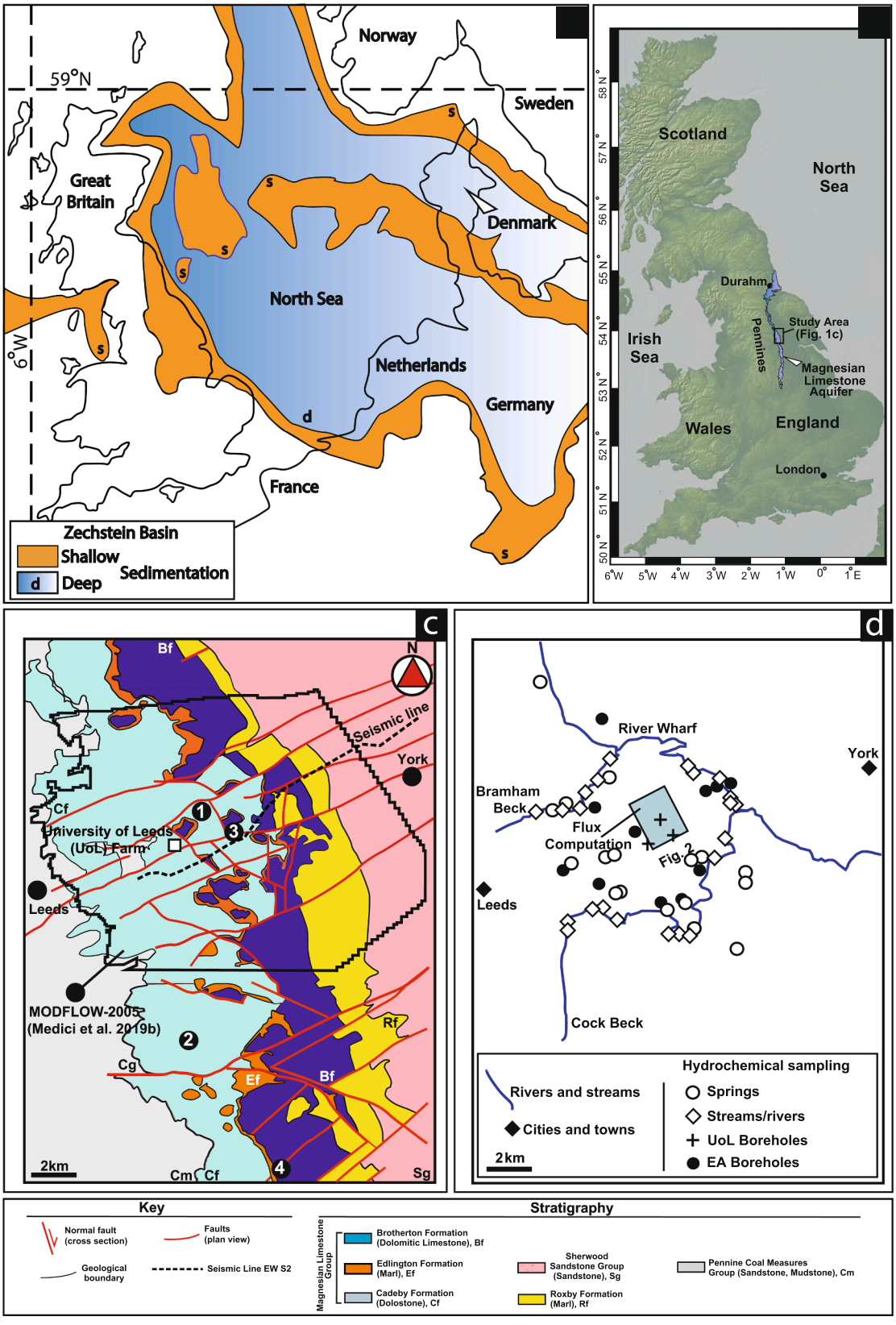

Fig. 1. The study site of the UoL Farm in the area of Leeds and York and the dolostone aquifer-unit of the Cadeby Formation. (a) The Permian Zechstein Basin and deposition of the shallow water deposits of the Cadeby Formation (from Mawson and Tucker, 2009); (b) Great Britain with location of the study area (basemap from GeoMapApp); (c) Map of the bedrock lithology with the location of the UoL Farm site, transect for computation of nitrate-DOC mass fluxes and MODFLOW-2005 model of the study area (Medici et al., 2019b); (d) Location of sampled streams, springs and boreholes.

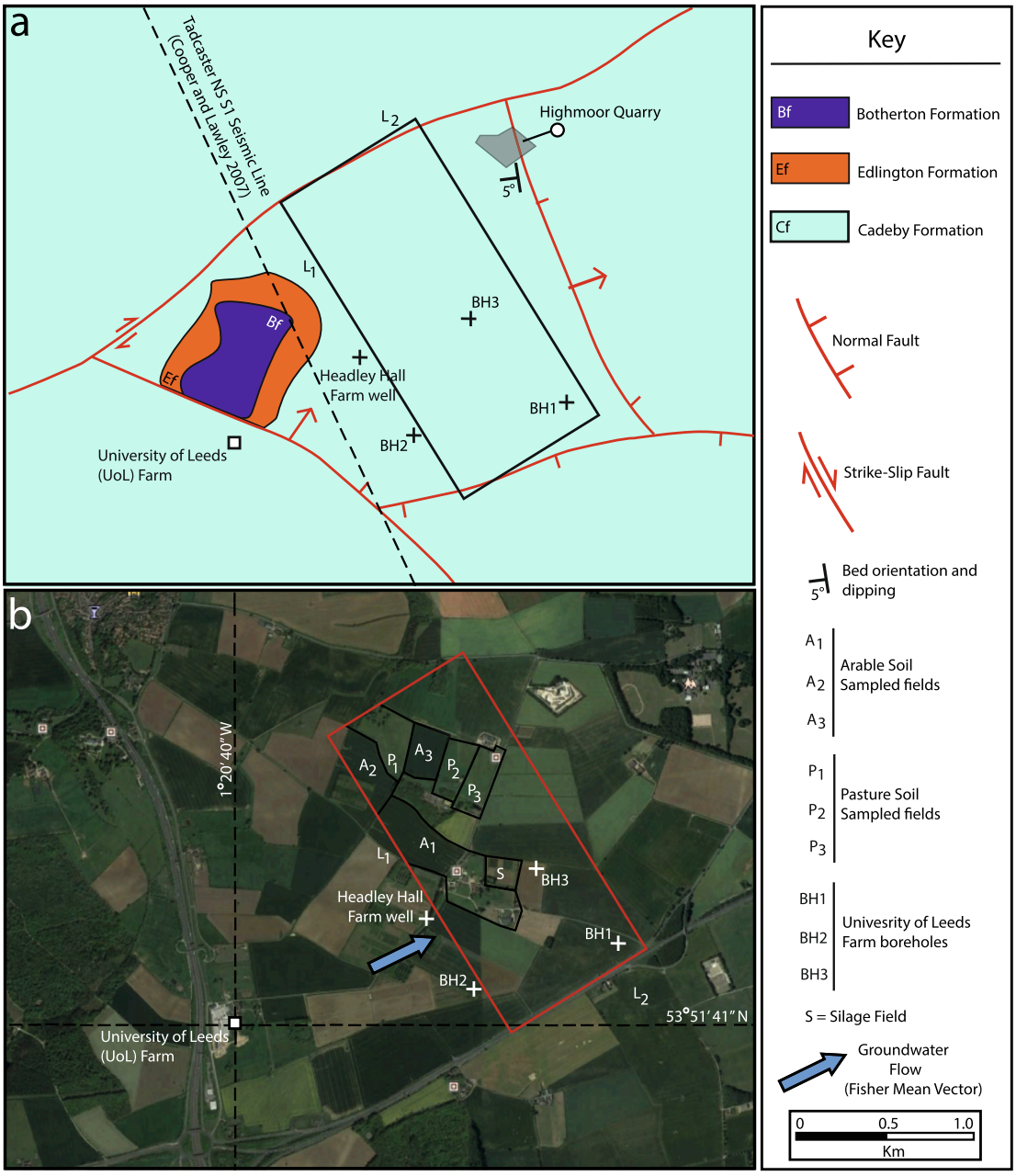

Fig. 2. Study site and detail of the transect. (a) Bedrock geology and studied boreholes, (b) Sampling points used for computation of nitrate-DOC mass fluxes.

orogenesis results in the gentle dip (<5° towards E) of the Permo-Mesozoic deposits in the study area (Figs. 1c, d, 2a; Murphy, 2000).

Boreholes drilled in non-faulted sections of the Cadeby Formation show high angle joints (dip 50°–80°) which cross-cut the bedding parallel fractures (Medici et al., 2019a). Cavities of karstic origin up to 0.6 m large were detected in correspondence of fault zones in the study area (Cooper and Lawley, 2007; Medici et al., 2019b). Vuggy porosity was detected at the field site in cores drilled in the vadose zone (Murphy, 2000; Murphy and Cordingley, 2010). Discontinuity surveys indicate 0.7 and 0.3 mm average mechanical apertures for sub-vertical joints and bedding plane, respectively (Medici et al., 2019b). Note that, availability of a seismic survey, cores and quarry outcrops allows good spatial constraints on geological formations and presence of faults in the UoL Farm area (Fig. 2a; Cooper and Lawley, 2007).

2.2. Land use and hydrogeology

The aquifer-unit of the Cadeby Formation is unconfined at the UoL Farm site due to the presence of only ~1 m thick Quaternary cover. The soil above the dolostone is a well-drained, loamy, calcareous brown earth type from the Aberford series of Calcaric Edoleptic Cambisols, and ranges in depth from 0.5 to 0.9 m (Holden et al., 2019). This soil type occurs extensively across the UK on gently sloping Permian and Jurassic Limestone and is mainly used for arable farming. The farm is comprised of 294 ha, the majority (264 ha) of which is arable with the remainder under grass. The arable fields have been in continuous cultivation and cropping since 1994 using a rotation of winter wheat (×2), spring or winter barley and oilseed rape, with the periodic inclusion of vining peas or potatoes. The grass fields are used for sheep grazing and some are cut for silage up to twice per year. Approximately 150 kg N ha^{-1} is applied to the cereal crops as fertiliser in spring with an additional 40 kg N ha^{-1} applied in the autumn as pig slurry after harvest. The grass fields receive

100–130 kg N ha^{-1} as fertiliser in spring and an additional 50 kg N ha^{-1} from pig slurry after silage harvest in June (Holden et al., 2019; Ward, 2020). The UoL Farm is distinct from the immediate surrounding agricultural land in that it applies pig slurry to both the arable fields and pasture fields as it has indoor and outdoor herds of pigs.

Below the soil, groundwater flow occurs in the saturated zone of the Cadeby Formation. This dolostone aquifer of Permian age is characterized by interquartile interval ranges for intergranular hydraulic conductivity and porosity which are 2.9×10^{-4} to 0.9×10^{-3} m/day and 8.5 to 18.7%, respectively (Allen et al., 1997). Flow occurs essentially in correspondence of fractures, i.e. evidenced by the large difference between permeability from pumping and core plug tests ($K_{well\text{-}test}/K_{core\text{-}plug} \sim 10^4$; see Fig. 3). Groundwater flow is more vigorous in correspondence of normal faults and here the bedrock is heavily karstified and fault traces are characterized by alignment of springs and streams that are located 3–4 km away from the study site (Fig. 1c). Fluid temperature and electrical conductivity are in the range of 9°–10° and 80–110 mS/m respectively according to the probes installed in the boreholes of the UoL Farm (Medici et al., 2019a). Flow rate ranges of springs and streams are 0.1–1 m^3/s and 0.1–4 m^3/s, respectively (Aldrick, 1978).

Slug tests in the Cadeby Formation conducted at the UoL site show hydraulic conductivities ranging from 0.07 to 2.89 m/day (Medici et al., 2019a). Notably, higher values of hydraulic conductivities (K = 0.83–2.89 m/day) from these tests characterize the first ~15 m below the water table (Medici et al., 2019a). Pumping tests indicate hydraulic conductivities ranging from 0.2 to 10 m/day with median values of 1.3 m/day across un-faulted areas for the Cadeby Formation of NE Yorkshire. The calibrated hydraulic conductivity for the Cadeby Formation from a MODFLOW-2005 steady state model for this area is 1.75 m/day (i.e. a similar value to those from pumping and shallow slug tests, see Fig. 3). Hence, the permeability of this dolostone aquifer primary comes from enhancement of fracture hydraulic aperture in first ~15 m below the water table (Medici et al., 2019a, 2019b). At such depths, hydraulic apertures (0.33–0.43 mm) have been computed applying the cubic law combining slug and fluid and televiewer logging at the study site (Medici et al., 2019a). This information on enhancement of hydraulic conductivity due to karstification has been incorporated in the MODFLOW-2005 flow model of the study site (Medici et al., 2019a, 2019b). Maximum fluctuations of the water table are typically 3.5 m during the hydrological year. As a consequence of the relatively small fluctuation of the water table, the model exclusively simulates steady state flow conditions and a constant rainfall recharge rate corresponding to the annual average of 0.134 m/year was applied.

3. Material and methods

3.1. Hydrochemistry

3.1.1. Water sampling

Water samples were collected from a variety of different sources, in order to characterize the hydrochemistry of the study site at and around the UoL Farm (field areas shown in Figs. 1b-d, 2a, b). These sources include; soil (n = 102), boreholes (n = 123, maximum depth 112 m), springs (n = 29) and streams (n = 22) (Fig. 1a-d). However, it should be noted that no springs or streams occur within the UoL research farm.

Soil water was sampled from both arable (n = 50) and pasture (n = 52) fields every two weeks between January and October 2017 using a 5-cm MacroRhizo (Eijkelkamp, Holland) soil moisture sampler (0.02 m diameter, 0.09 m length) resulting in a total of 102 samples. Six fields were studied; three fields were arable and three were improved permanent grassland (location of these fields A1-3 and P1-3 are shown in Fig. 2b). Soil water samples were collected at the depth intervals of 0.05–0.10 m and 0.35–0.40 m.

The boreholes are divided into two groups that penetrate the Cadeby Formation to different depths. Group 1 are boreholes installed by the UoL at the Farm site (BH1, BH2 and BH3, see Figs. 1d and 2b) where the water table is between 10 and 15 m below ground level (BGL). Group 1 boreholes are characterized by a diameter 0.20 m large at the UoL Farm. This group of boreholes were screened with 2.3–3 m long intervals

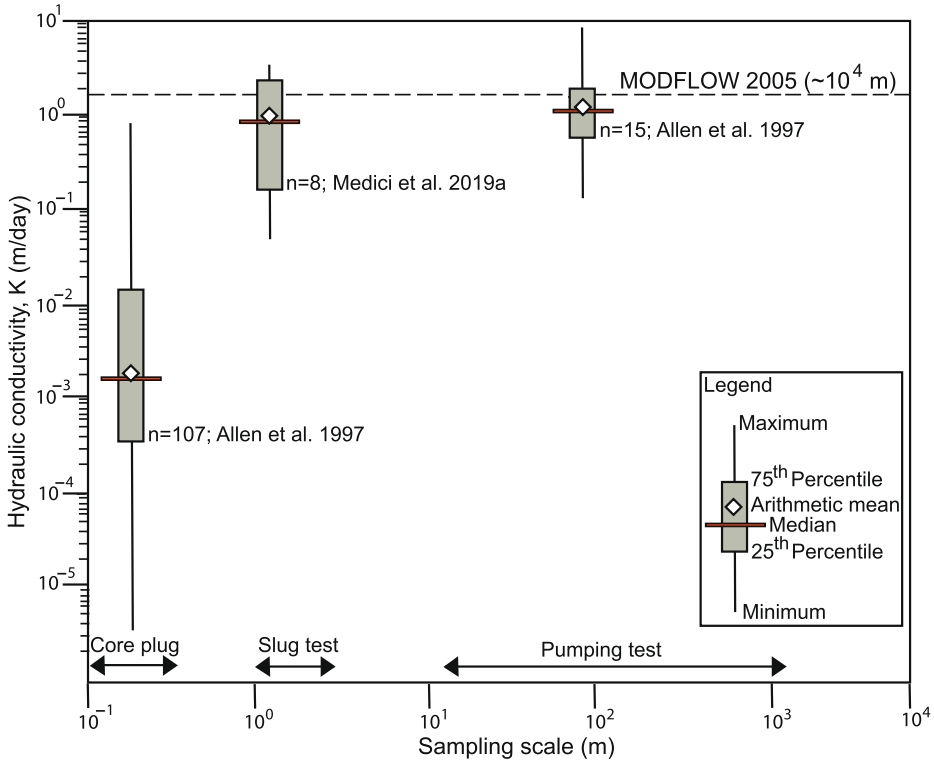

Fig. 3. Hydraulic conductivity vs. scale for the Cadeby Formation at the study site.

between 8 and 40 mBGL and were sampled 6 times from October 2017 to September 2018. Thus, groundwater samples were collected at multiple depths in each of the UoL boreholes. Group 2 are boreholes sampled by the Environment Agency of England (EA, see Fig. 1d) in the vicinity of the UoL Farm; these are typically deeper and are screened within the depth interval 15–112 mBGL and are characterized by diameters ranging from 0.15 and 0.60 m. In addition, the EA also collected water samples from springs and streams near the farm (Fig. 1d). The samples from springs, streams and Group 2 boreholes were collected two times per year by EA staff between 2006 and 2018.

3.1.2. Chemical analysis

Hydrochemical analysis of cations (Na^+, Mg^{2+}, K^+, Ca^{2+}, Mn^{2+}, Fe^{2+}, Al^{3+}), anions (Cl^-, SO_4^-, NO_3^-, HCO_3^-) and DOC have been undertaken in streams, springs and groundwater within the dolostone of the Cadeby Formation to characterize the Critical Zone of the UoL Farm area (field area shown in Figs. 1b, d; 2a, b). Soil water samples were analysed using a Mettler Toledo S20 pH meter, Horiba LAQUAtwin conductivity meter, and a Skalar San ++ continuous flow analyser for NO_3^- concentrations. Dissolved organic and inorganic carbon (DOC and DIC, respectively) concentrations were determined using an Analytik Jena Multi N/C 2100C combustion analyser.

The temperature, electrical conductivity and pH of all groundwater, spring, and stream samples was measured using a 6PFCE Ultrameter 2 (Myron L Company). Groundwater alkalinity was measured by titration in the field. Calibration of probes was carried out at the beginning of each working day and maintenance of calibration was assessed prior to each measurement. All groundwater samples were filtered through a 0.25 μm pore membrane into a 50 mL bottle in the field using a syringe; a 10% nitric acid was added to those 50 mL bottles intended for cation analyses. All groundwater, spring and stream water samples were stored at 4° C in the fridge prior to laboratory analyses (following Piper, 1953). Major anions (Cl^-, SO_4^{2-}, NO_3^-) and cations (Na^+, Mg^{2+}, K^+, Ca^{2+}, Mn^{2+}, Fe^{2+}, Al^{3+}) were determined using an ICS0 ion chromatographer and ICP, respectively. Charge balance errors were calculated and ranged from 0.1 up to 4.5%, which suggests good quality data.

Dissolved organic carbon (DOC) concentrations in all groundwater samples was calculated from the difference between total dissolved carbon (DC) and dissolved inorganic carbon (DIC), which was measured by a Multi N/C Analyser. A comparison was made between the dissolved inorganic carbon concentration from the laboratory analysis and that derived from the alkalinity titration in the field; concentrations were very similar (+/− 2.5% discrepancy) indicating good sample preservation.

3.2. Calculation of nitrate and DOC mass fluxes

The Transect Method (*sensu* Goltz et al., 2007) was applied at the UoL Farm to determine the mass flux of DOC and nitrate that represent the principal groundwater quality indicators and contaminants in a KCZ (Goldscheider and Drew, 2014; Figs. 2, 4). The transect was applied avoiding faults where the bedrock can be assumed homogeneous (Fig. 2a). The described approach represents the first application, as far as we are aware, of the Transect Method to a Farm that we refer to as TMF. Given the concentration of the chemical species in groundwater, C_i, the advective groundwater mass flux, M_{gw}, is calculated as:

$$M_{gw} = C_{gw} \times Q_{gw} \quad (1)$$

where Q is the groundwater flux defined by the Darcy's law as the product of the hydraulic conductivity (K) and the hydraulic gradient (i) and transect area (A_2). Note that in the case of the transect area defined in Fig. 2, the hydraulic gradient (annual arithmetic average, 0.0236) is known from the monitoring of the three boreholes at the UoL Farm and the aquifer hydraulic conductivity (arithmetic mean, 1.1 m/day; Fig. 3) from slug tests (Medici et al., 2019a). Slug test values representative of the horizontal hydraulic conductivity show arithmetic mean > geometric mean > median > harmonic mean. The arithmetic mean was selected for use in this study, representing the highest mean, because the most highly conductive layers dominate horizontal flow at the field site (Medici et al., 2019a).

Given the contaminant concentration (C_{sw}) of the specific chemical specie in soil water collected at the base of the soil profile at 0.35–0.45 m depth[1], the contaminant mass flux from the land surface through area A_1 (Fig. 4) is then defined as:

$$M_{inf} = C_{sw} \times Q_{inf} \quad (2)$$

where Q_{inf} is the product of the recharge rate (i.e. precipitation minus evapotranspiration) and the area A_1. The annual average recharge rate used to calculate the hydrological flux from the land surface (Q_{inf}) is 0.134 m/year derived from the calibrated MODFLOW-2005 regional groundwater model previously used at the field site (Medici et al., 2019b). The use of unique recharge value is supported by the selection of a transect area that is overlain by uniform ~0.5 m thick well drained calcareous soil above a relatively homogenous bedrock, avoiding fault zones (Fig. 2a).

A theoretical 3D block (see Figs. 1d, 2 and 4) has been created with the longer side oriented parallel to the annual groundwater Fisher mean vector (azimuth 68°; Medici et al., 2019a). The area used to compute the upstream groundwater flux (Q_{gw}) is defined by the parallelepiped side, L1 (Fig. 2) and the aquifer saturated thickness of 30 m estimated by the British Geological Survey core logs (Cooper and Lawley, 2007, Fig. 4).

Our analysis assumes that the total mass flux (M_{mix}) of the two species leaving the transect area within groundwater is given by the sum of the groundwater flux entering the transect area (M_{gw}) and that infiltrating through the soil zone (M_{inf}) (Fig. 4). Median values of DOC and nitrate concentration (C_i) were calculated from the dataset available in the area of the transect to apply equations (1) and (2). Concentrations in groundwater from the Headley Hall Farm and BH2 borehole and the soil water concentrations collected at 0.40 mBGL (Figs. 2b, 4) were used to define C_{gw} and C_{sw} respectively. Note that, DOC and nitrate concentrations from Hadley Hall Farm and BH2 were selected due the upstream position of these boreholes with respect to the other boreholes of the UoL Farm, BH1 and BH3 (Fig. 2b). The Headley Farm is the shallowest borehole that the Environment Agency sample in the study area and is screened at the same depth interval of BH1, BH2 and BH3. The Headley Farm, BH1, BH2 and BH3 boreholes are all characterized by a 0.20 m diameter.

To test the validity of the TMF, the modelled DOC and nitrate mass fluxes were converted into concentrations dividing by the surface plus groundwater flux, Q_{mix} ($Q_{gw} + Q_{in}$). This conversion allows comparison with the measured concentration values acquired from the UoL Farm boreholes.

4. Results

4.1. Aquifer physiochemical properties

The mean, range and standard deviation for electrical conductivity, fluid temperature and pH for the different source waters are shown in Table 1. The mean pH of all the surface and groundwater samples was 7.4° and ranged from 6.5° to 8.0° (Fig. 1d). Mean fluid temperature collected from all the different sources of water was 10.0° and ranged from 9.2° up to 19.9 °C (Fig. 1d). Electrical conductivity of the water samples displayed a wide range; from 140 up to 1558 μS/cm (n = 276).

Comparison between the different sources of water indicates

[1] Samples were collected at the base of the soil zone to obtain concentrations of nitrate and DOC below the zone of potential denitrification and differential bacterial activity within the soil.

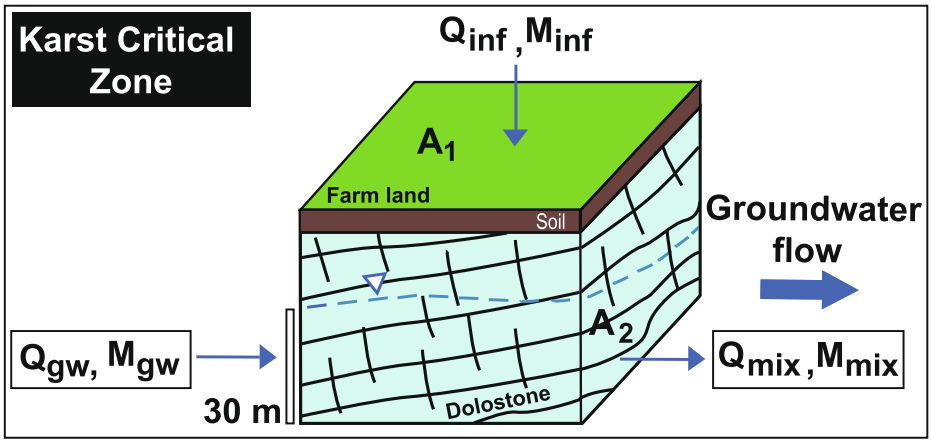

Fig. 4. Theoretical 3D block for calculation of nitrate and DOC mass fluxes at the study site.

Table 1
Fluid temperature, electrical conductivity and pH arithmetic mean, range and standard deviation (σ) for the UoL and the EA boreholes, springs, streams and arable and pasture fields.

Data source	pH Mean; Range; σ	Fluid Temperature (℃) Mean; Range; σ	Electrical Conductivity (μS/cm) Mean; Range; σ
University of Leeds boreholes	7.3; 7.0–7.6; 0.1	10.2; 9.2–11.4; 0.11	880; 775–1086; 95
EA Borehole	7.9; 7.4–8.0; 0.2	18.1; 16.2–19.9; 3.4	890; 660–1170; 167
Spring	7.2; 7.0–7.7; 0.2	12.1; 9.8–19.3; 2.3	972; 640–1558; 281
Stream	7.4; 7.4–7.9; 0.2	13.9; 10.5–17.9; 1.5	817; 443–1154; 817
Arable Soil	7.6; 6.9–7.9; 0.3	N/A	670; 280–1070; 208
Pasture Soil	7.1; 6.5–8.0; 0.9	N/A	540; 140–790; 93

similarity in the pH and conductivity values between the shallow (0–40 mBGL) boreholes of the UoL and the soil waters from the arable and pasture fields as well as the springs. Overlap of electrical conductivity, fluid temperature and pH ranges indicates a good degree of hydraulic connectivity between the soil, shallow saturated aquifer zone and springs (Table 1). In contrast, pH, fluid temperature and electrical conductivity are higher in the groundwater sampled at depth from the EA boreholes, indicating a lower degree of hydraulic connectivity with all sources of surface water. Fluid temperature and electrical conductivity from the stream samples were more scattered compared to the other water sources, probably due to contribution of external surface water sources and atmospheric control on surface water temperature (Table 1).

The groundwater of the Cadeby Formation, shows a Ca^{2+}-Mg^{2+} bicarbonate-type composition (Fig. 5). The order of abundance is $Ca^{2+}>Mg^{2+}>Na^{+}>Al^{3+}>Mn^{2+}>Fe^{2+}$ and $HCO^{3-}>SO4^{2-}>Cl^{-}>NO_3^-$ for cations and anions, respectively. Binary diagrams, which provide information on the chemical processes occurring in the Cadeby Formation, are illustrated in Fig. 6a-c. The Mg^{2+}-Ca^{2+} binary diagram shows positive correlation, which lies above the 1:1 ratio (Fig. 6a). This trend is due to the higher abundance of more highly soluble calcite with respect to dolomite (60% $CaCO_3$, 40% Mg_2CO_3) in the Cadeby Formation of Yorkshire (Lott and Cooper, 2005). Na^{+}-Cl^{-} regression lines (Fig. 6b) are parallel to the 1:1 ratio which indicates dissolution of halite, which is most likely related to dissolution of evaporites within the Edlington Formation. The latter evaporitic formation is juxtaposed against the Cadeby Formation by normal faults that behave as hydraulic connectors (see Figs. 1c, 2).

Similarly, SO_4^{2-}-Ca^{2+} linear regression (Fig. 6c) indicates gypsum dissolution from the evaporitic strata of the Edlington Formation (Moussa et al., 2014; Re et al., 2017). Note that, the SO_4^{2-}-Ca^{2+} regression lines do not superimpose exactly on the 1:1 line for gypsum dissolution due to additional Ca^{2+} input from dissolution of calcite in the Magnesian Limestone Group. Springs show a higher concentration of Ca^{2+} with respect to groundwater and streams (Fig. 6a, c).

The World Health Organization (WHO) drinking water quality limit for nitrate (50 mg/L) is breached in many of the EA boreholes, springs and streams, and in the pasture soil water samples (Fig. 7). The nitrate 75th percentile is also above the WHO limit in all the UoL boreholes (Fig. 8).

Overall, nitrate concentration shows medians which are respectively above and below the WHO limit in the groundwater sampled from the UoL shallow (15–40 mBGL) boreholes versus those sampled from the deeper (20–112 mBGL) EA boreholes. Note, no consistent variation in nitrate concentrations with depth was recognized from the multiple depth intervals (8–40 mBGL) in the UoL boreholes. Nitrate concentrations however substantially decrease at greater depths >40 mBGL seen in samples from the EA boreholes (Fig. 7). Nitrate concentrations in the springs are very similar to that of the shallow UoL boreholes, whereas, nitrate concentrations in streams are lower than those in both the UoL boreholes and springs (and the upper percentile lies below the WHO limit, Fig. 7).

Nitrate concentrations in the soil water from the pasture fields are similar to those in the groundwater from the UoL boreholes (Fig. 7). This similarity suggests that leaching from these pasture soils which are upstream of the farm boreholes (see Fig. 2) are a major nitrate source for groundwater of the studied Permian dolostone. Indeed, nitrate concentration is higher in pasture soil where livestock is present compared with arable land exclusively used to grow crops as shown in Fig. 7. Nitrate concentrations are lower in streams compared with soil water and groundwater as illustrated in the box plot in Fig. 7. This concentration difference may arise from dilution of the groundwater baseflow component of streamflow by freshwater runoff that is generated in correspondence of the low permeability units of the Pennine Coal Measure Group in the western sector of the study site (Fig. 1; Aldrick, 1978).

Ranges, interquartile ranges and median concentration (C) of DOC are shown in Fig. 9. Similar and highest DOC concentrations were observed in the soil water from the pasture (C_{median} = 13.0 mg/L) and arable (C_{median} = 11.0 mg/L) fields. Concentrations of DOC in the saturated zone of the aquifer were considerably smaller, with median values of 5.5 mg/L in groundwater from the UoL boreholes (15 to 35 mBGL) and 0.5 mg/L from the deeper (>40 mBGL) EA boreholes. Here, the

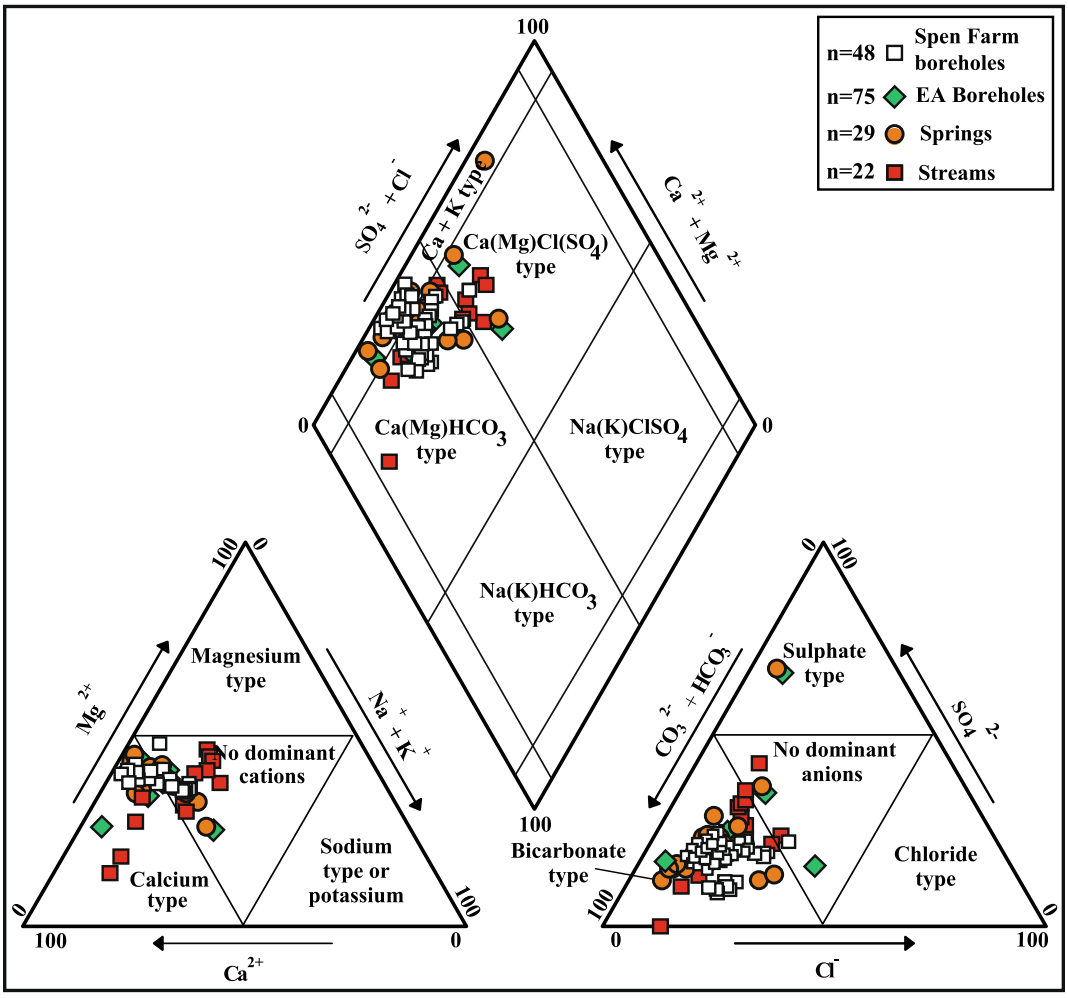

Fig. 5. Piper diagram for water samples from boreholes, springs and streams.

observed pattern of DOC in soil water, shallow and deeper groundwater is consistent with infiltration from both the farm arable and pasture soils providing increased DOC to shallow (15–40 mBGL) groundwater. DOC concentrations observed at the shallower depth (8–40 mBGL) intervals sampled via the UoL Farm boreholes do not show evident depth variations. However, DOC varies seasonally from 1.0 up to 13.8 mg/L (Fig. 6) and shows a wider seasonal variation than the other solute chemical species, with higher concentrations observed in the spring-summer period from late April to June.

4.2. DOC and nitrate mass fluxes

Mass fluxes of nitrate and DOC were modelled applying the TMF to a theoretical 3D block in the area of the UoL Farm (Figs. 2, 4). The inputs and outputs for this method are illustrated in Table 2 for 'background or inflowing' groundwater (Q_{gw}, M_{gw}), infiltrating recharge water (Q_{inf}, M_{inf}), and exiting groundwater (Q_{mix}, M_{mix}), in terms of DOC and nitrate fluxes. The initial step for this computation is the definition of the fluxes of recharge and groundwater flow (see Fig. 4). The recharge flux (Q_{inf}) is the product of the annual average recharge rate from the calibrated MODFLOW-2005 model (see Fig. 1c) and land surface area (A_1) applied at the top of the 3D block that represents a portion of the land surface (see Fig. 4). The groundwater flux (Q_{gw}) is calculated from the annual average hydraulic gradient (0.0236) and arithmetic mean hydraulic conductivity (1.1 m/day) from slug tests applied to the saturated thickness of aquifer unit (Medici et al., 2019a). The sum of these two contributions (Q_{inf}, Q_{gw}) provides the outflowing groundwater flux (Q_{mix}) of 2292 m^3/day for the selected transect (Fig. 2b; Table 2).

Mass fluxes of nitrate and DOC were modelled from Q_{in}, Q_{out} by applying equations (1) and (2) (Table 2). Median concentrations of nitrate (Figs. 7, 8) and DOC (Fig. 9) from land surface and inflowing groundwater flow are assumed to be those from soil water (median of all arable and pasture measurements) and from the EA Headley Hall Farm and BH2 boreholes that are located upstream with respect to the other two UoL boreholes (Fig. 2b).

The infiltrating mass fluxes (M_{inf}) are 4526 and 10454 kg yr^{-1} for DOC and nitrate, respectively according to the proposed model. The transect is 200 ha and therefore infiltration mass fluxes can be expressed as 23 and 52 kg yr^{-1} ha^{-1} for DOC and nitrate, respectively to enable comparison at the UoL as well as other farm areas across the world.

Applied nitrogen inputs from arable and pasture field are 190 and 180 kg yr^{-1} ha^{-1}, respectively. 52 kg yr^{-1} ha^{-1} of NO_3^- corresponds to 12 kg yr^{-1} ha^{-1} of N flux. This N value of flux is derived from natural recharge and reaches the water table. Hence, ~6% of applied nitrogen infiltrates in the saturated part of the aquifer.

The outflowing nitrate flux derived from equations (1) and (2) is 45202 kg yr^{-1} and contains the inflowing mass flux, M_{gw} (34748 kg yr^{-1}; Table 2) as well as that infiltrating from the transect. DOC outflowing mass flux is 5146 kg yr^{-1} as shown in Table 2. Notably, model outputs show that $M_{inf} < M_{gw}$ for nitrate. This hydrochemical scenario contrasts the modelled DOC mass fluxes that indicate $M_{inf} \gg\gg M_{gw}$ (Table 2). The UoL Farm appears therefore to be an evident point source of DOC and a more mild nitrate-polluter.

To test the validity of the TMF, the modelled DOC and nitrate mass

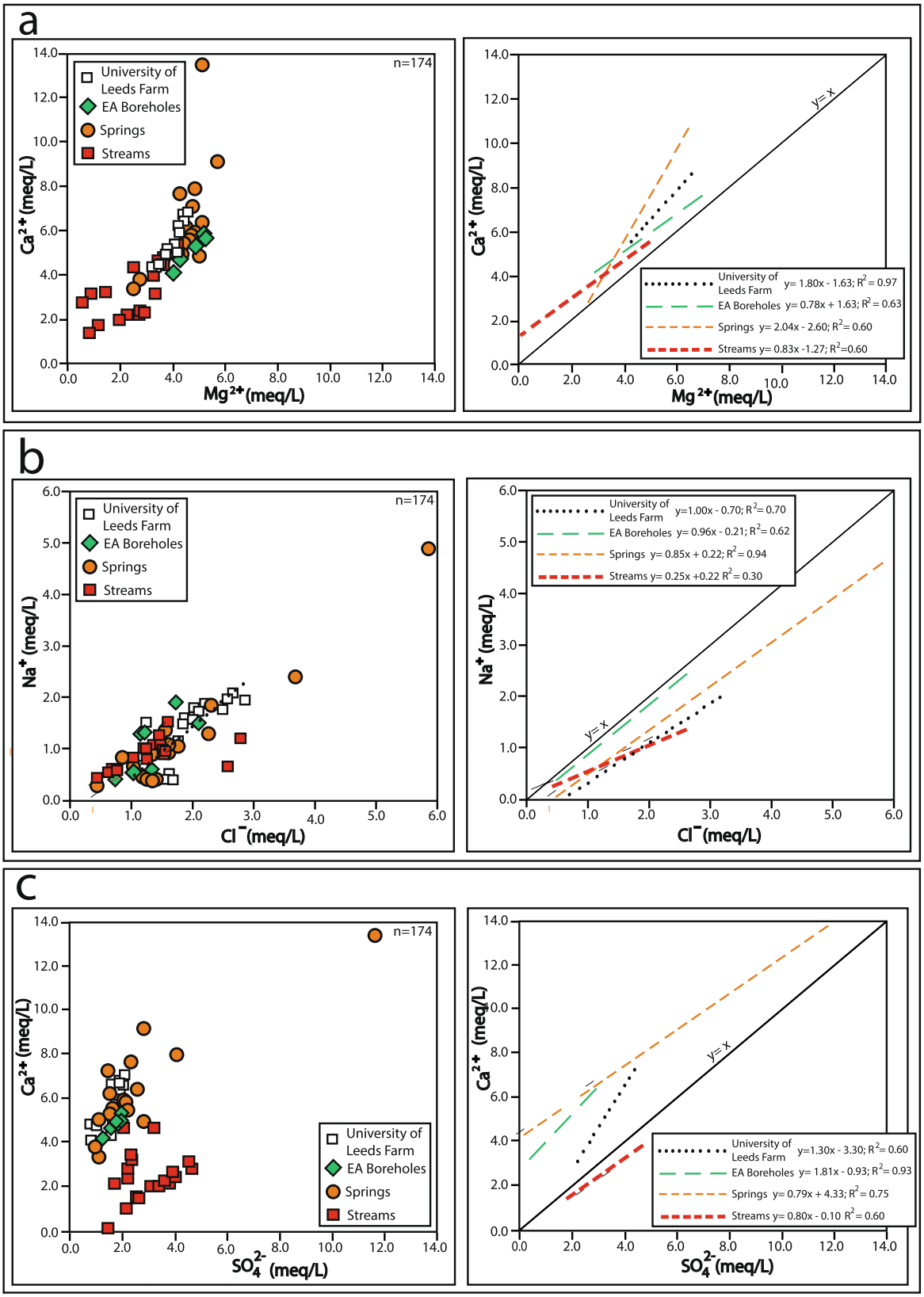

Fig. 6. Binary diagrams for springs, boreholes and streams; **a** Cl^{-}-Na^{+}, **b** Mg^{2+}-Ca^{2+}, **c** SO^{4-}-Ca^{2+}.

fluxes are converted into modelled downstream concentrations by dividing the groundwater flux leaving the site downstream boundary, Q_{mix} (2292 m^3/day). The modelled concentrations for DOC and nitrate are shown as dashed lines in Figs. 7 and 8 (for nitrate) and 9 (for DOC). While concentrations at the downstream boundary were not measured directly, these modelled concentrations can be compared to the measured concentration in groundwater at the BH1 and BH3 receptors (see Fig. 2b).

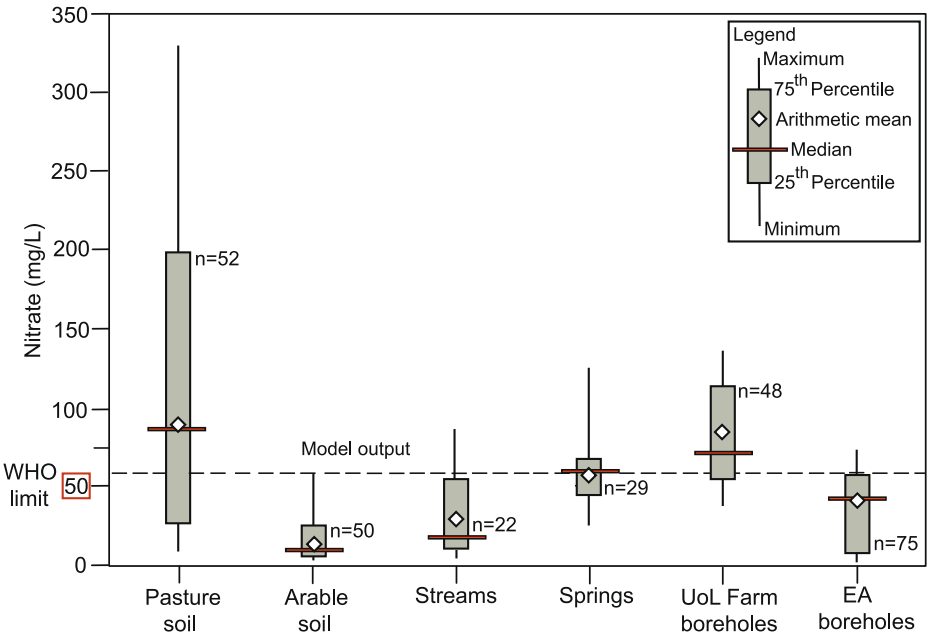

Fig. 7. Model output vs. concentrations of nitrates in samples from soil moisture, springs, streams and boreholes.

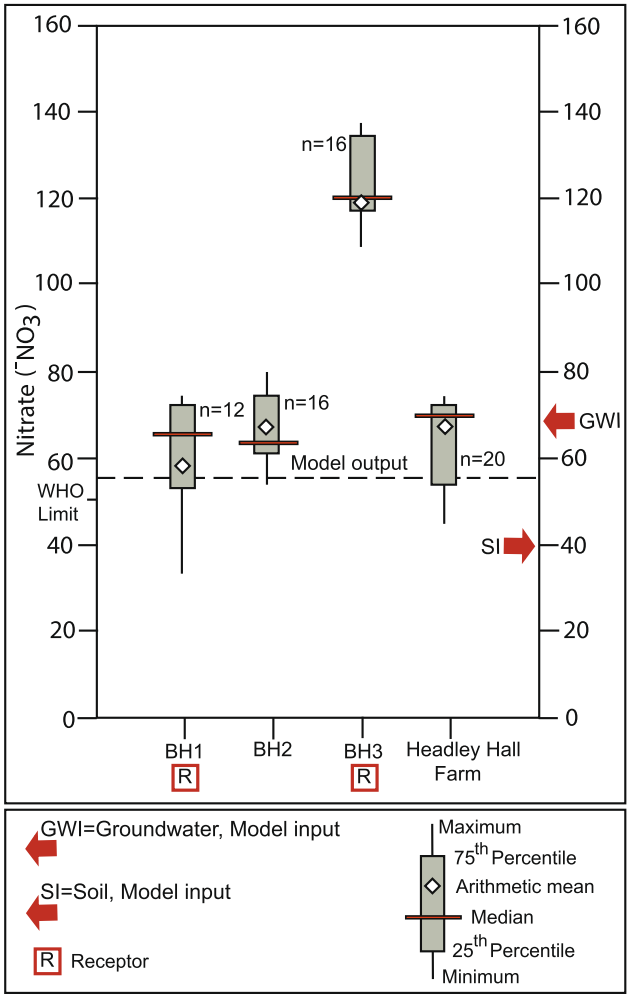

Fig. 8. Model output vs. concentrations of nitrate in the EA Headley Farm wells, and BH1, BH2 and BH3 boreholes of the UoL Farm.

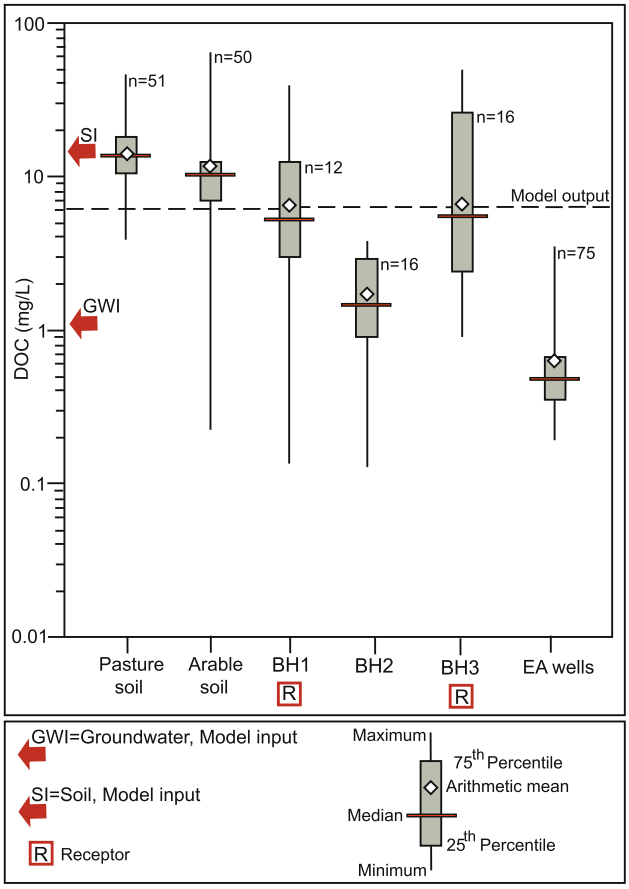

Fig. 9. Model output vs. concentrations of DOC in samples from soil moisture, springs and boreholes.

The modelled nitrate (54.0 mg/L) concentration from the transect calculation falls within the interquartile range (53.0–71.5 mg/L) of nitrate for BH1 (Fig. 8). However, BH3 nitrate concentrations lies above the model output of 54.0 mg/L, possibly due to the proximity of a silage

Table 2
Input and output parameters for computation of mass fluxes of DOC and nitrate.

Water Fluxes (Input)		Q_{inf} (m^3/day)	Q_{gw} (m^3/day)	Q_{mix} (m^3/day)
		734	1558	2292
Mass Fluxes (Output)	Chemical Specie	M_{in}	M_{gw}	M_{mix}
	Nitrate (kg yr^{-1})	10,454	34,748	45,202
	DOC (kg yr^{-1})	4526	620	5146

field that has received pig slurry (Figs. 2b, 8). The model also highlights that if the median soil water nitrate concentration was reduced by 40% from 40.0 mg/L to 24.0 mg/L the modelled out-flowing nitrate concentration in groundwater would fall below the 50 mg/L that represents the limit imposed by the World Health Organization. Thus agricultural practices in the arable and pasture fields need to be modified to reduce soil water nitrate concentrations by this amount.

The modelled DOC (6.2 mg/L) concentration from transect calculation fall within the interquartile ranges of DOC (3.0–10.3 and 2.2–11.7 mg/L for BH1 and BH3, respectively) in the two receptors of the UoL (Fig. 9). Notably, the model outputs closely match the arithmetic average of BH1 and BH3 boreholes for DOC. These results support validity of the presented TMF approach (Figs. 7–9; Table 2).

5. Discussion

The influence of soil-derived nitrate and DOC on groundwater quality was studied in a dolomitic KCZ at UoL Experimental Farm. From a hydrochemical point of view, analyses reveal a baseline Ca^{2+}-Mg^{2+} bicarbonate-type water that represents the typical composition of dolostone aquifers (Seyhan et al., 1985; Barbieri et al., 2005; Xanke et al., 2015). Similarly, the range of nitrate (Fig. 7) and DOC (Fig. 9) concentrations from soil and groundwater indicate a high degree of hydraulic connectivity between these two elements, as commonly reported for a KCZ (Jourde et al., 2018); this is discussed further in section 5.1.

Hydraulic conductivity values of the Cadeby Formation increase from the core-log to the scale of the field site. Groundwater flow models find calibration with values that overlap those of pumping tests (Fig. 3; Schulze-Makuch et al., 1999; Gleeson et al., 2011). This physical feature is typical for moderately karstified aquifers. As a consequence of the common physiochemical features of the studied aquifer, this research shows how physical hydrogeological parameters from modelling groundwater flow can be combined with hydrochemical analyses to develop approaches for modelling contaminant fluxes via KCZs under farmland.

5.1. Aquifer vulnerability

Nitrate and DOC are good indicators of aquifer vulnerability to contamination in areas dedicated to intense agriculture (Ducci, 2010; Wachniew et al., 2016). DOC is an important parameter from the viewpoint of water quality at farm sites in karst areas (Moral et al., 2008; Goldscheider and Drew, 2014; Koit et al., 2020). One reason for its importance is that DOC forms complexes with hydrophobic organic contaminants released by pesticides facilitating their transport (Wang et al., 2004, 2018).

In this paper, we have used DOC and nitrate concentrations in surface, soil and groundwater to characterize the flux of NO_3^- and DOC through the Permian dolostone of the Cadeby Formation (see conceptual model illustrated in Fig. 10) and in doing so identified the most vulnerable depth interval of the aquifer. Pasture soil waters have much higher concentrations of nitrate than arable soil waters (the latter show values below the WHO drinking water limit). Nitrate concentrations decrease with depth from the pasture soil water to the shallow (<~40 mBGL) groundwater, and at depths >40 mBGL nitrate concentrations are even lower; mostly below the WHO drinking water limit (Fig. 7). DOC concentrations are similar in arable and pasture soil waters, with lower concentrations in shallow (0–40 mBGL) groundwater (Figs. 9, 10). Note that, DOC also decreases at depths >40 mBGL in the

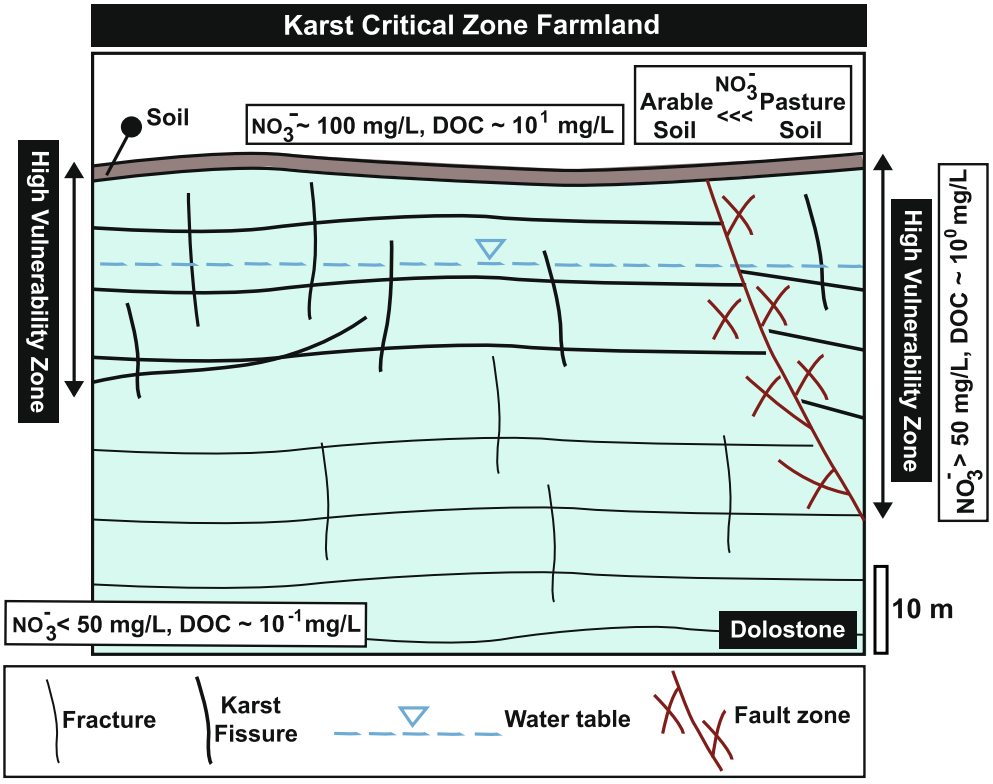

Fig. 10. Hydrogeological conceptual scheme of the KCZ of at the UoL Farm site.

deep aquifer. Other studies have also reported a sharp decrease in both nitrate and DOC concentrations with depth in the KCZ in agricultural areas (Foster et al., 1982; Geyer et al., 1992).

Our research suggests that the zone of maximum aquifer vulnerability is in the first 40 m below the soil surface. This zone partially includes the most conductive (K = 0.83–2.89 m/day) part of the aquifer that is in the depth interval 0–25 mBGL as indicated by multi-level slug tests (Medici et al., 2019a). However, karstification is much more pervasive in correspondence of normal fault zones intercepted in the area of the relatively deep abstraction wells (Fig. 1c). These faults are more conductive in borehole tests (K_{median} = 35 m/day; n = 7; Allen et al., 1997) and characterized by much faster modelled groundwater velocities (3000–5500 m/day; Medici et al., 2019b) as typical in faulted dolostone aquifer portions (Bauer et al., 2016). Intense karstification persists up to 40 m depth in correspondence of these tectonized zones justifying a relatively deep vulnerable zone (see Fig. 10).

5.2. TMF and solute contaminant transport

Mass fluxes of nitrate and DOC arising from agricultural practices at the farm, including pig slurry spreading, were modelled using the TMF applying the rainfall recharge from the calibrated regional MODFLOW-2005 flow model (Fig. 3; Medici et al., 2019b). Modelled mean concentrations of DOC and nitrate in groundwaters down-gradient of the site are within the range of those measured (Figs. 7–9; Table 2). The modelled nitrogen mass flux (12 kg ha^{-1} yr^{-1}) driven by rainfall recharge indicates that ~6% of applied nitrogen (from pig slurry plus mineral fertilisers) reaches the saturated part of the aquifer; a value that is in the expected range of infiltration fractions (5–50%) (Liao et al., 2012; Green et al., 2018). Literature also supports the modelled values of nitrate flux in farmland. Indeed, nitrogen fluxes applied to crops is ~10^1 kg ha^{-1} yr^{-1} in areas of the world dedicated to intense agriculture (Messer and Brezonik, 1983; Jordan et al., 1998; Green et al., 2018). The TMF therefore provides a reliable tool to compute solute mass fluxes leaving a farm site via the groundwater pathway. Note that at this field site denitrification below the soil zone is unlikely to be significant, which means that the assumption of the TMF that nitrate is conserved within the aquifer is valid. This scenario is related to low groundwater temperature (9°–10°) that typically inhibits denitrification (Rivett et al., 2008). Furthermore, measured groundwater flow velocities which are very high (50–250 m/day, Medici et al., 2019a) and hence residence times in the aquifer are too low to allow significant denitrification, as proposed by other authors for similar aquifers across the world (Moon et al., 2006; Goldscheider and Drew, 2014; Hartmann et al., 2014; Yang et al., 2020).

Nitrate and DOC concentrations in soil and groundwater are known to vary temporally and spatially due to variations in hydrology, soil physical and chemical properties, crop rotation and fertilizer inputs (Sieling et al., 1997; Lord et al., 1999; Williams and Gresham, 2000). In recent years, there has been concerted efforts to improve the nitrogen use efficiency of both inorganic fertilisers and manure/slurry applications in order to help reduce nitrate leaching. In 2000, Chambers et al. (2000) reported that about 50% of pig and poultry manures are applied in the autumn (August-October) to cereal stubble in the UK. However, they also found that highest nitrate losses occurred following the application of slurry to winter cereals in the autumn. This practice is applied at the UoL Farm and here more nitrate is available for leaching. Pig slurry application is going to change at the studied farm in the near future. In fact, in recent years, advice to UK farmers has focussed on getting them to switch from autumn to spring applications for high readily-available-N manures and slurry (Chambers et al., 2000; Ball Coelho et al., 2006).

This research develops the application of the Transect Method, previously used for prediction of impacts of industrial sources on groundwater quality, to other point sources of contamination such as farms. Previous applications of the Transect Method focused on prediction of contaminant mass fluxes and concentration at industrial field sites related to release of chlorinated pollutants and heavy metals (Verreydt et al., 2012, 2013; Padgett et al., 2017). Here we show that the Transect Method can be used to define mass fluxes and hence concentrations of contaminants in groundwater. The approach provides an indication of whether a particular point source (in this case a farm where pig slurry spreading occurs) has a significant impact on the contamination load in groundwater. In our case, the results show that the farm has a significant impact on groundwater DOC concentrations, and to a lesser extent nitrate concentrations (see Table 2). This scenario is related to surrounding farms use of inorganic fertilisers so regional groundwater nitrate concentrations are already relatively high, whereas pig slurry spreading is less common in the immediate vicinity of the UoL Farm. In fact, pig slurry is practiced at this farm because the indoor pig unit at the farm provides a ready supply.

The TMF could also be used to define the boundary conditions for solute transport models (e.g., Goltz et al., 2007) for prediction of downstream impacts for example at well abstractions at the study site. Thus, the future modelling of reactive contaminant transport at the UoL Farm must primarily focus on the first and highly vulnerable ~40 m below the ground using different concentrations of nitrate and DOC in soil and groundwater (Fig. 10).

6. Conclusions

Nitrate and DOC are considered two key chemical species that determine water quality in the CZ in karstic environments. Here, we propose an approach to demonstrate how the combination of hydrochemical analyses of different water sources from multiple depths, combined with physical groundwater flow model characterisation allows prediction of mass fluxes of DOC and nitrate from farmland via the groundwater pathway. A robust hydraulic characterisation reveals the mechanisms of solute transport and facilitates future modelling scenarios. In this paper, the KCZ of the Permian dolostone of NE Yorkshire (NE England, UK) has been used and the Transect Method applied to compute nitrate and DOC mass fluxes at the study site (the University of Leeds Farm, Yorkshire, UK). This methodology is used to predict the impacts of farm activity on concentrations of pollutant species in groundwater. The transect approach is here applied for the first time to a farm-source of contaminations where pig slurry is applied in the autumn when leaching losses are highest to both cereal crops, and pasture fields (post cutting for silage). The use of this methodology was validated by comparing the modelled concentrations of DOC and nitrate with measured concentrations in groundwater. The results show that the farm activity influences the 'background' concentrations of both DOC and nitrate in groundwater. The influence on DOC is most marked, because this farm uses pig slurry rather than only inorganic fertilisers, which is more common for the surrounding farms.

The hydrochemical analysis of groundwater highlights that the zone of highest vulnerability to contamination to the first ~40 m below the ground surface is due to higher concentrations of nitrate and DOC being observed in this zone. This zone also had high hydraulic conductivity of karst fissures and conduits in the first ~15 m below the water table that most likely vertically extends to greater depths in faulted areas. Hence, future modelling of KCZ contaminant transport should primarily focus in the first ~40 m below the ground.

Following this research, we envisage to export the TMF that combines a groundwater model-derived recharge, baseline soil water and groundwater analyses and computation of mass fluxes to support conceptualization and modelling of contaminant transport in other karst areas.

CRediT authorship contribution statement

G. Medici: Writing - original draft, Conceptualization, Methodology, Software. **P. Baják:** Software, Writing - review & editing. **L.J. West:**

Conceptualization, Methodology, Writing - review & editing, Supervision. **P.J. Chapman:** Conceptualization, Methodology, Writing - review & editing. **S.A. Banwart:** Supervision, Conceptualization.

Declaration of Competing Interest

The authors declare that they have no known competing financial interests or personal relationships that could have appeared to influence the work reported in this paper.

Acknowledgements

The work represents a synthesis of 15 years of hydrochemical and hydrological research at the UoL Farm. Funding is acknowledged from the Natural Environment Research Council via the CZO: Using Critical Zone Science-Peri-Urban Agriculture in China and the Soil Security Programme grants, and the Faculty of Environment via funding to support MSc Student Dissertation research. Hence, the support of MSc students Zeyu Ao and Christian Walker that have collected some of the field data was especially appreciated.

Edward Wrathmell (Environment Agency of England) gave assistance with hydrochemical licensing issues and provision of data under licence. We also thank Rachael Spraggs (University of Leeds) for arranging data access licensing. We are grateful to managers and operators at the UoL Farm for supporting our work, particularly George Sorensen for planning borehole instrumentation, Richard Grayson, Sarah Hunt and Martin Lappage for collecting the soil water samples and David Ashley for analysing them. However, Rachel Gasior analysed the groundwater samples from the UoL boreholes. This research also benefited from discussions with Kent Keller (Washington State University) and Beth Parker (University of Guelph), regarding transport of toxic compounds in the Karst Critical Zone. Finally, guidance from Editor-in-Chief Corrado Corradini and comments from three anonymous reviewer have substantially improved the manuscript.

References

Aldrick, R.J., 1978. The hydrogeology of the Magnesian Limestones in Yorkshire between the River Wharfe and the River Aire. Quart. J. Engineer. Geol. Hydrogeol. 11 (2), 193–201.

Allen-King, R.M., Grathwohl, P., Ball, W.P., 2002. New modeling paradigms for the sorption of hydrophobic organic chemicals to heterogeneous carbonaceous matter in soils, sediments, and rocks. Advan. Water Resour. 25 (8–12), 985–1016.

Anderson, S.P., Hinckley, E.L., Kelly, P., Langston, A., 2014. Variation in critical zone processes and architecture across slope aspects. Procedia Earth Planet. Sci. 10, 28–33.

Allen, D.J., Brewerton, L.M., Coleby, B.R., Gibbs, M.A., Lewis, A., MacDonald, S.J., Wagstaff, A.T., Williams, L.J., 1997. The Physical Properties of Major Aquifers in England and Wales. Technical Report WD/97/34, 157-287. British Geological Survey, Nottingham, England (UK).

Ball Coelho, B.R., Roy, R.C., Bruin, A.J., 2006. Nitrogen recovery and partitioning with different rates and methods of sidedressed manure. Soil Sci. Soc. Am. J. 70 (2), 464–473.

Banwart, S., Bernasconi, S.M., Bloem, J., Blum, W., Brandao, M., Brantley, S., Chabaux, F., Duffy, C., Kram, P., Lair, G., Lundin, L., 2011. Soil processes and functions in critical zone observatories: hypotheses and experimental. Vadose Zone J. 10 (3), 974–987.

Banwart, S.A., Bernasconi, S.M., Blum, W.E., de Souza, D.M., Chabaux, F., Duffy, C., Kercheva, M., Krám, P., Lair, G.J., Lundin, L., Menon, M., 2017. Soil functions in Earth's critical zone: key results and conclusions. Adv. Agron. 142, 1–27.

Barbieri, M., Boschetti, T., Petitta, M., Tallini, M., 2005. Stable isotope (2H, 18O and 87Sr/86Sr) and hydrochemistry monitoring for groundwater hydrodynamics analysis in a karst aquifer (Gran Sasso, Central Italy). Appl. Geochem. 20 (11), 2063–2081.

Bauer, H., Schröckenfuchs, T.C., Decker, K., 2016. Hydrogeological properties of fault zones in a karstified carbonate aquifer (Northern Calcareous Alps, Austria). Hydrogeol. J. 24 (5), 1147–1170.

Bicalho, C.C., Batiot-Guilhe, C., Seidel, J.L., Van Exter, S., Jourde, H., 2012. Geochemical evidence of water source characterization and hydrodynamic responses in a karst aquifer. J. Hydrol. 450, 206–218.

Borović, S., Terzić, J., Pola, M., 2019. Groundwater quality on the adriatic karst Island of Mljet (croatia) and its implications on water supply. Geofluids 2019. https://doi.org/10.1155/2019/5142712.

Brantley, S.L., Eissenstat, D.M., Marshall, J.A., Godsey, S.E., Balogh-Brunstad, Z., Karwan, D.L., Papuga, S.A., Roering, J., Dawson, T.E., Evaristo, J., Chadwick, O., 2017. Reviews and syntheses: on the roles trees play in building and plumbing the critical zone. Biogeoscience 17, 14(22).

Chambers, B.J., Smith, K.A., Pain, B.F., 2000. Strategies to encourage better use of nitrogen in animal manures. Soil Use Manage. 16, 157–166.

Cooper, A.H., Lawley, R.S., 2007. Tadcaster Magnesian Limestone 3-D Borehole Interpretation and Cross-sections Study. British Geological Survey, Nottingham, England (UK).

Defra, 2002. The Government's strategic review of diffuse water pollution from agriculture in England and Wales. Department for Environment, Food and Rural Affairs, London.

Dong, X., Cohen, M.J., Martin, J.B., McLaughlin, D.L., Murray, A.B., Ward, N.D., Flint, M. K., Heffernan, J.B., 2018. Ecohydrologic processes and soil thickness feedbacks control limestone-weathering rates in a karst landscape. Chemical Geol. 118774.

Ducci, D., 2010. Aquifer Vulnerability assessment methods: the non-independence of parameters problem. J. Water Resour. Protect. 2 (4).

Emblanch, C., Zuppi, G.M., Mudry, J., Blavoux, B., Batiot, C., 2003. Carbon 13 of TDIC to quantify the role of the unsaturated zone: the example of the Vaucluse karst systems (Southeastern France). J. Hydrol. 279 (1–4), 262–274.

Falcone, R.A., Falgiani, A., Parisse, B., Petitta, M., Spizzico, M., Tallini, M., 2008. Chemical and isotopic (δ18O‰, δ2H‰, δ13C‰, 222Rn) multi-tracing for groundwater conceptual model of carbonate aquifer (Gran Sasso INFN underground laboratory–central Italy). J. Hydrol. 357 (3–4), 368–388.

Fezzi, C., Hutchins, M.G., Rigby, D., Bateman, I.J., Posen, P., Hadley, D., 2010. Integrated assessment of water framework directive nitrate reduction measures. Agric. Econ. 41 (2), 123–134.

Ford, D.C., Williams, P.W., 1989. Karst Geomorphology and Hydrology. Unwin Hyman, London (UK).

Foster, S.S.D., 1976. The vulnerability of British groundwater resources to pollution by agriculture leachates. MAFF Tech. Bull. 32, 159–165.

Geyer, D.J., Keller, C.K., Smith, J.L., Johnstone, D.L., 1992. Subsurface fate of nitrate as a function of depth and landscape position in Missouri Flat Creek watershed, USA. J. Contam. Hydrol. 11 (1–2), 127–147.

Goldscheider, N., Drew, D., 2014. Methods in Karst hydrogeology: IAH: International Contributions to Hydrogeology. Crc Press, p. 26.

Goltz, M.N., Kim, S., Yoon, H., Park, J., 2007. Review of groundwater contaminant mass flux measurement. Environ. Engineer. Res. 12 (4), 176–193.

Goss, M.J., Barry, D.A.J., Rudolph, D.L., 1998. Contamination in Ontario farmstead domestic wells and its association with agriculture: 1. Results from drinking water wells. J. Contam. Hydrol. 32 (3–4), 26–293.

Gleeson, T., Smith, L., Moosdorf, N., Hartmann, J., Dürr, H.H., Manning, A.H., van Beek, L.P., Jellinek, A.M., 2011. Mapping permeability over the surface of the Earth. Geophys. Res. Lett. 38 (2).

Green, S.M., Dungait, J.A., Tu, C., Buss, H.L., Sanderson, N., Hawkes, S.J., Xing, K., Yue, F., Hussey, V.L., Peng, J., Johnes, P., 2019. Soil functions and ecosystem services research in the Chinese karst Critical Zone. Chem. Geol. 527, 119107.

Green, C.T., Liao, L., Nolan, B.T., Juckem, P.F., Shope, C.L., Tesoriero, A.J., Jurgens, B.C., 2018. Regional variability of nitrate fluxes in the unsaturated zone and groundwater, Wisconsin, USA. Water Resour. Res. 54 (1), 301–322.

Hartmann, A., Goldscheider, N., Wagener, T., Lange, J., Weiler, M., 2014. Karst water resources in a changing world: review of hydrological modeling approaches. Rev. Geophys. 52 (3), 218–242.

Hill, M.E., Stewart, M.T., Martin, A., 2010. Evaluation of the MODFLOW-2005 conduit flow process. Groundwater 48 (4), 549–559.

Holden, J., Grayson, R.P., Berdeni, D., Bird, S., Chapman, P.J., Edmondson, J.L., Firbank, L.G., Helgason, T., Hodson, M.E., Hunt, S.F.P., Jones, D.T., 2019. The role of hedgerows in soil functioning within agricultural landscapes. Agricultur. Ecosyst. Environm. 273, 1–12.

Huang, W., Yu, H., Weber Jr, W.J., 1998. Hysteresis in the sorption and desorption of hydrophobic organic contaminants by soils and sediments: 1. A comparative analysis of experimental protocols. J. Contam. Hydrol. 31 (1–2), 129–148.

Huebsch, M., Horan, B., Blum, P., Richards, K.G., Grant, J., Fenton, O., 2013. Impact of agronomic practices of an intensive dairy farm on nitrogen concentrations in a karst aquifer in Ireland. Agric. Ecosyst. Environ. 179, 187–199.

Hutchins, M.G., 2012. What impact might mitigation of diffuse nitrate pollution have on river water quality in a rural catchment? J. Environ. Manage. 109, 19–26.

Jiang, Z., Zhang, C., Qin, X., Pu, J., Bai, B., 2019. Structural features and function of the Karst critical zone. Acta Geol. Sin. 93, 109–112.

Jordan, T.E., Weller, D.E., Correll, D.L., 1998. Denitrification in surface soils of a riparian forest: Effects of water, nitrate and sucrose additions. Soil Biol. Biochem. 30 (7), 833–843.

Jourde, H., Massei, N., Mazzilli, N., Binet, S., Batiot-Guilhe, C., Labat, D., Steinmann, M., Bailly-Comte, V., Seidel, J.L., Arfib, B., Charlier, J.B., 2018. SNO KARST: A French network of observatories for the multidisciplinary study of critical zone processes in karst watersheds and aquifers. Vadose Zone J. 17 (1).

Keller, C.K., 2019. Carbon exports from terrestrial ecosystems: a critical-zone framework. Ecosyst. 22 (8), 1691–1705.

Koit, O., Barberá, J.A., Marandi, A., Terasmaa, J., Kiivit, I.K., Martma, T., 2020. Spatiotemporal assessment of humic substance-rich stream and shallow karst aquifer interactions in a boreal catchment of northern Estonia. J. Hydrol. 580, 12423.

Kogovsek, J., Petric, M., 2014. Solute transport processes in a karst vadose zone characterized by long-term tracer tests (the cave system of Postojnska Jama, Slovenia). J. Hydrol. 519, 1205–1213.

Kuntz, B.W., Rubin, S., Berkowitz, B., Singha, K., 2011. Quantifying solute transport at the shale hills critical zone observatory. Vadose Zone J. 10 (3), 843–857.

Lastennet, R., Mudry, J., 1997. Role of karstification and rainfall in the behavior of a heterogeneous karst system. Environ. Geol. 32 (2), 114–123.

Lerch, R.N., Groves, C.G., Polk, J.S., Miller, B.V., Shelley, J., 2018. Atrazine transport through a Soil-Epikarst system. J. Environ. Qual. 47 (5), 1205–1213.
Lian, B., Yuan, D., Liu, Z., 2011. Effect of microbes on karstification in karst ecosystems. Chin. Sci. Bullet. 56 (35), 3743–3747.
Liao, L., Green, C.T., Bekins, B.A., Böhlke, J.K., 2012. Factors controlling nitrate fluxes in groundwater in agricultural areas. Water Resour. Resear. 48 (6) https://doi.org/10.1029/2011WR011008.
Lord, E.I., Johnson, P.A., Archer, J.R., 1999. Nitrate sensitive areas: a study of large scale control of nitrate loss in England. Soil Use Manage. 15 (4), 201–207.
Lott G.K., Cooper, A.H., 2005 The building limestones of the Upper Permian, Cadeby Formation (Magnesian Limestone) of Yorkshire. Report IR/05/048, British Geological Survey, Nottingham (UK).
Mahler, B., Massei, N., 2007. Anthropogenic contaminants as tracers in an urbanizing karst aquifer. J. Contam. Hydrol. 91 (1–2), 81–106.
Mawson, M., Tucker, M., 2009. High-frequency cyclicity (Milankovitch and millennial-scale) in slope-apron carbonates: Zechstein (Upper Permian), North-east England. Sedimentology 56 (6), 1905–1936.
Medici, G., West, L.J., Mountney, N.P., 2016. Characterizing flow pathways in a sandstone aquifer: tectonic vs sedimentary heterogeneities. J. Contam. Hydrol. 194, 36–58.
Medici, G., West, L.J., Banwart, S.A., 2019a. Groundwater flow velocities in a fractured carbonate aquifer-type: implications for contaminant transport. J. Contam. Hydrol. 222, 1–16.
Medici, G., West, L.J., Chapman, P.J., Banwart, S.A., 2019b. Prediction of contaminant transport in fractured carbonate aquifer types: a case study of the Permian Magnesian Limestone Group (NE England, UK). Environ. Sci. Pollut. Res. 26 (24), 24863–24884.
Mellander, P.E., Jordan, P., Wall, D.P., Melland, A.R., Meehan, R., Kelly, C., Shortle, G., 2012. Delivery and impact bypass in a karst aquifer with high phosphorus source and pathway potential. Water Resear. 46 (7), 2225–2236.
Messer, J., Brezonik, P.L., 1983. Comparison of denitrification rate estimation techniques in a large, shallow lake. Water Resear. 17 (6), 631–640.
Moon, H.S., Nam, K., Kim, J.Y., 2006. Initial alkalinity requirement and effect of alkalinity sources in sulfur-based autotrophic denitrification barrier system. J. Environ. Eng. 132 (9), 971–975.
Moral, F., Cruz-Sanjulián, J.J., Olías, M., 2008. Geochemical evolution of groundwater in the carbonate aquifers of Sierra de Segura (Betic Cordillera, southern Spain). J. Hydrol. 360 (1–4), 281–296.
Moussa, A.B., Mzali, H., Zouari, K., Hezzi, H., 2014. Hydrochemical and isotopic assessment of groundwater quality in the Quaternary shallow aquifer, Tazoghrane region, north-eastern Tunisia. Quatern. Int. 338, 51–58.
Murphy, P.J., 2000. The karstification of the Permian strata east of Leeds. Proc. York. Geol. Soc. 53 (1), 25–30.
Murphy, P.J., Cordingley, J.N., 2010. Mass movement caves in northern England. Proc. Univ. Bristol Spelaeol. Soc. 25 (1), 105–112.
Odling, N.E., Gillespie, P., Bourgine, B., Castaing, C., Chiles, J.P., Christensen, N.P., Fillion, E., Genter, A., Olsen, C., Thrane, L., Trice, R., 1999. Variations in fracture system geometry and their implications for fluid flow in fractured hydrocarbon reservoirs. Petrol. Geosci. 5 (4), 373–384.
Padgett, M.C., Tick, G.R., Carroll, K.C., Burke, W.R., 2017. Chemical structure influence on NAPL mixture nonideality evolution, rate-limited dissolution, and contaminant mass flux. J. Contam. Hydrol. 198, 11–23.
Panno, S.V., Hackley, K.C., Hwang, H.H., Kelly, W.R., 2001. Determination of the sources of nitrate contamination in karst springs using isotopic and chemical indicators. Chem. Geol. 179, 113–128.
Peyraube, N., Lastennet, R., Denis, A., 2012. Geochemical evolution of groundwater in the unsaturated zone of a karstic massif, using the PCO2–SIc relationship. J. Hydrol. 430, 13–24.
Peyraube, N., Lastennet, R., Denis, A., Malaurent, P., 2013. Estimation of epikarst air PCO2 using measurements of water δ13CTDIC, cave air PCO2 and δ13CCO2. Geochim. Cosmochim. Acta 118, 1–17.
Piper A.M., 1953 A graphic procedure in the geochemical interpretation of water analysis. Groundwater Note 12. United States Geological Survey. Reston, Virginia (USA).
Re, V., Sacchi, E., Kammoun, S., Tringali, C., Trabelsi, R., Zouari, Daniele, S., 2017. Integrated socio-hydrogeological approach to tackle nitrate contamination in groundwater resources. The case of Grombalia Basin (Tunisia). Sci. Total Environ. 593, 664–676.
Rivett, M.O., Buss, S.R., Morgan, P., Smith, J.W.N., Bemment, C.D., 2008. Nitrate attenuation in groundwater: a review of biogeochemical controlling processes. Water Res. 42, 4215–4232.
Ryan, M., Meiman, J., 1996. An examination of short-term variations in water quality at a karst spring in Kentucky. Groundwater 34 (1), 23–30.
Schulze-Makuch, D., Carlson, D.A., Cherkauer, D.S., Malik, P., 1999. Scale dependency of hydraulic conductivity in heterogeneous media. Groundwater 37 (6), 904–919.
Seyhan, E., Van De Griend, A.A., Engelen, G.B., 1985. Multivariate analysis and interpretation of the hydrochemistry of a dolomitic reef aquifer, northern Italy. Water Resour. Res. 21 (7), 1010–1024.
Sieling, K., Günther-Borstel, O., Hanus, H., 1997. Effect of slurry application and mineral nitrogen fertilization on N leaching in different crop combinations. J. Agric. Sci. 128 (1), 79–86.
Siemens, J., Haas, M., Kaupenjohann, M., 2003. Dissolved organic matter-induced denitrification in subsoils and aquifers? Geoderma 113, 253–271.
Smith, D.B., Harwood, G.M., Pattison, J., Pettigrew, T.H., 1986. A revised nomenclature for Upper Permian strata in eastern England. Geol. Soc. London Spec. Publ. 22, 9–17.
Sullivan, T.P., Gao, Y., Reimann, T., 2019. Nitrate transport in a karst aquifer: Numerical model development and source evaluation. J. Hydrol. 573, 432–448.
Torresan, F., Fabbri, P., Piccinini, L., Dalla Libera, N., Pola, M., Zampieri, D., 2020. Defining the hydrogeological behavior of karst springs through an integrated analysis: a case study in the Berici Mountains area (Vicenza, NE Italy). Hydrogeol. J. 1–19.
Tremosa, J., Debure, M., Narayanasamy, S., Redon, P.O., Jacques, D., Claret, F., Robinet, J.C., 2020. Shale weathering: a lysimeter and modelling study for flow, transport, gas diffusion and reactivity assessment in the critical zone. J. Hydrol. 124925.
Tucker, M.E., 1991. Sequence stratigraphy of carbonate-evaporite basins: models and application to the Upper Permian (Zechstein) of northeast England and adjoining North Sea. J. Geol. Soc. 148 (6), 1019–1036.
Xanke, J., Goeppert, N., Sawarieh, A., Liesch, T., Kinger, J., Ali, W., Hötzl, H., Hadidi, K., Goldscheider, N., 2015. Impact of managed aquifer recharge on the chemical and isotopic composition of a karst aquifer, Wala reservoir, Jordan. Hydrogeol. J. 5, 1027–1040.
Verreydt, G., Annable, M.D., Kaskassian, S., Van Keer, I., Bronders, J., Diels, L., Vanderauwera, P., 2013. Field demonstration and evaluation of the Passive Flux Meter on a CAH groundwater plume. Environ. Sci. Pollut. Resear. 20 (7), 4621–4634.
Verreydt, G., Van Keer, I., Bronders, J., Diels, L., Vanderauwera, P., 2012. Flux-based risk management strategy of groundwater pollutions: the CMF approach. Environ. Geochem. Health 34 (6), 725–736.
Wachniew, P., Zurek, A.J., Stumpp, C., Gemitzi, A., Gargini, A., Filippini, M., Rozanski, K., Meeks, J., Kværner, J., Witczak, S., 2016. Toward operational methods for the assessment of intrinsic groundwater vulnerability: a review. Crit. Rev. Env. Sci. Tec. 46 (9), 827–884.
Wakida, F.T., Lerner, D.N., 2005. Non-agricultural sources of groundwater nitrate: a review and case study. Water Resear. 39 (1), 3–16.
Wang, Z., Chen, M., Zhang, L., Wang, K., Yu, X., Zheng, Z., Zheng, R., 2018. Sorption behaviors of phenanthrene on the microplastics identified in a mariculture farm in Xiangshan Bay, southeastern China. Sci. Total Environ. 628, 1617–1626.
Wang, H., Magesan, G.N., Bolan, N.S., 2004. An overview of the environmental effects of land application of farm effluents. New Zeal. J. Agr. Res. 47 (4), 389–403.
Wang, L., Stuart, M.E., Lewis, M.A., Ward, R.S., Skirvin, D., Naden, P.S., Collins, A.L., Ascott, M.J., 2016. The changing trend in nitrate concentrations in major aquifers due to historical nitrate loading from agricultural land across England and Wales from 1925 to 2150. Sci. Total Environ. 542, 694–705.
Ward, K., 2020. Slurry analysis results at the University of Leeds Farm and surrounding areas. NRM Laboratories, Report 84722.
Weber Jr, W.J., Huang, W., Yu, H., 1998. Hysteresis in the sorption and desorption of hydrophobic organic contaminants by soils and sediments: 2. Effects of soil organic matter heterogeneity. J. Contam. Hydrol. 31 (1–2), 149–165.
Williams, T.M., Gresham, C.A., 2000. Nitrogen accumulation and changes in nitrate leaching after 4 years of intensive forest culture on marginal agricultural land. NZ Forestry Sci. 30, 266–279.
Worthington, S.R., Smart, C.C., Ruland, W., 2012. Effective porosity of a carbonate aquifer with bacterial contamination: Walkerton, Ontario, Canada. J. Hydrol. 464, 517–527.
Yang, P., Wang, Y., Wu, X., Chang, L., Ham, B., Song, L., Groves, C., 2020. Nitrate Sources and biogeochemical processes in karst underground rivers impacted by different anthropogenic input characteristics. Environ. Pollut. 265, 114835.
Zhang, Z., Chen, X., Soulsby, C., 2017. Catchment-scale conceptual modelling of water and solute transport in the dual flow system of the karst critical zone. Hydrol. Process. 31 (19), 3421–3436.
Zhou, Q., Chen, L., Singh, V.P., Zhou, J., Chen, X., Xiong, L., 2019. Rainfall-runoff simulation in karst dominated areas based on a coupled conceptual hydrological model. J. Hydrol. 573, 524–533.